Evolution of solar wind turbulence during radial alignment of PSP with Solar Orbiter in December 2022

SH-226

Ashok Silwal[1], Lingling Zhao[1,2], Xingyu Zhu[2]

[1]Department of Space Science, University of Alabama in Huntsville, Huntsville, AL

[2]Center for Space Plasma and Aeronomic Research, University of Alabama in Huntsville, Huntsville, AL

THE UNIVERSITY OF ALABAMA IN HUNTSVILLE

CENTER FOR SPACE PLASMA & AERONOMIC RESEARCH

Introduction

- The solar wind is a turbulent flow of weakly collisional charged particles that originates in the outermost layer of the Sun's atmosphere, the solar corona, and expands radially into the heliosphere.
- Because of the background interplanetary magnetic field, the turbulence in the solar wind is anisotropic. The anisotropic energy cascade leads to the anisotropy of power level and spectral index, which is observed in the solar wind turbulence.
- One way to study the radial evolution of solar wind turbulence properties is to consider same plasma crossing two spacecrafts.

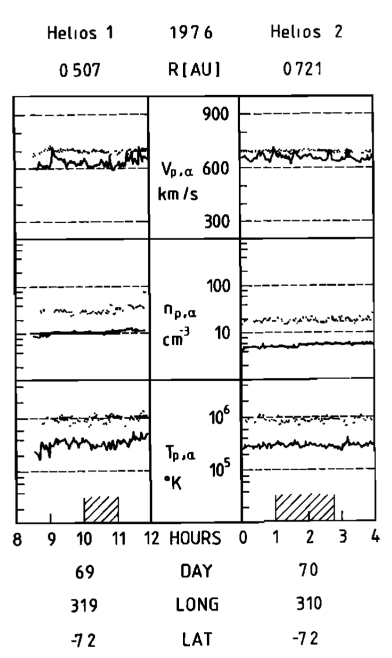

- Fast solar wind
- Prediction assuming a constant and radial propagation velocity
- Solar wind's expansion taken into account
- Helios Era: few studies, not very conclusive (large error bars, data gaps)

Fig. 1. Helios 1 and Helios 2 sampling same plasma parcel[1].

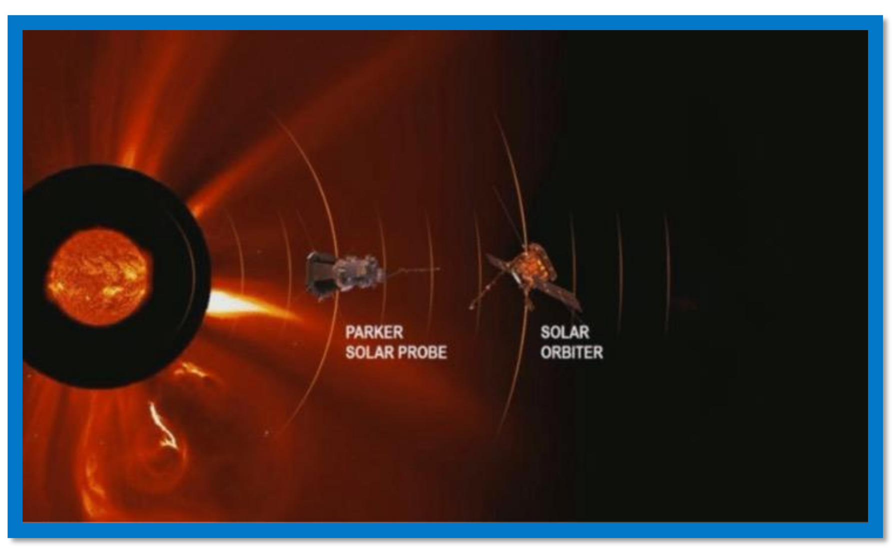

Fig. 2. Parker Solar Probe and Solar Orbiter. Image courtesy of NASA.

Goal: detect and study the same parcel of solar wind at different heliospheric distances from the Sun (**plasma line-up**)

Characterization of the solar wind radial evolution !

The recently launched missions Parker Solar Probe (PSP; **Fox et al. 2016**) and Solar Orbiter (SolO; **Müller et al. 2020**) provide an exciting and unprecedented opportunity to obtain rare measurements of the same plasma parcel through the radial alignment of these two spacecraft can provide insight into the actual evolution of waves, turbulence, and heating under different conditions.

Data and and Line-up Configuration

We use publicly available measurements of PSP and Solar Orbiter from 2022 December 10 through 2022 December 20.

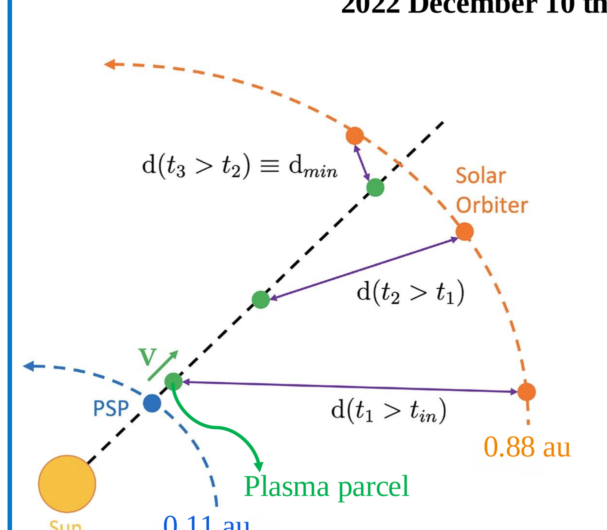

Fig. 3. Simplified schematic of the propagation method for a purely radial plasma speed. Adapted from **Berriot et al. 2024**.

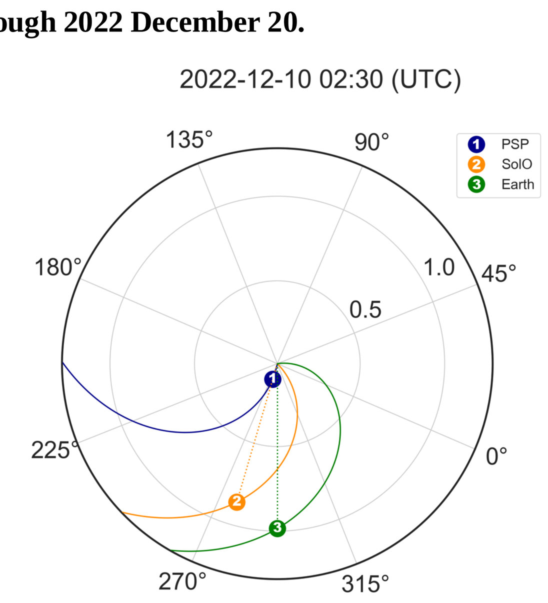

Fig. 4. PositionS of PSP and SolO during the radial alignment event of December 10, 2022. Credit: **Solar-MACH**.

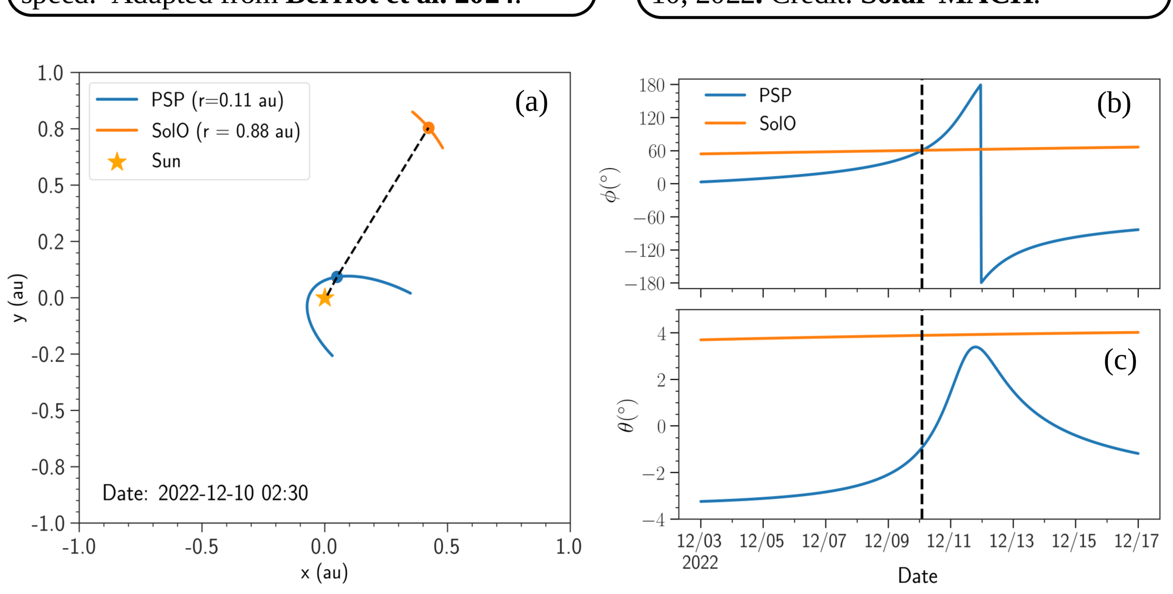

Fig. 5. Panel (a) shows the positions (dots) and trajectories (lines) of PSP (blue) and Solar Orbiter (orange) in the ecliptic plane from December 3-17, 2022. Panels (b) and (c) display the longitude (φ) and latitude (θ) of PSP (blue) and Solar Orbiter (orange). The vertical dashed black line marks the spacecraft coalignment time t_0.

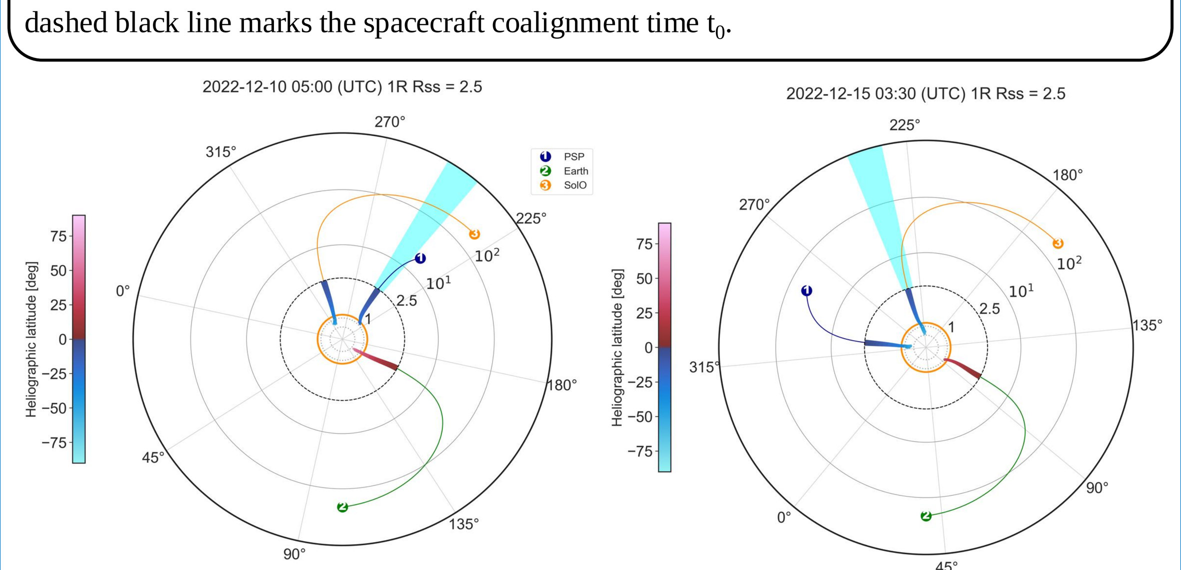

Fig. 6. Potential Field Source Surface (PFSS) backmapping for the selected time intervals to confirm whether the plasma observed by PSP and SolO comes from the same source region at the Sun. The yellow circle represents the photosphere at one solar radius. The source surface height has been adjusted to $2.5R_{\odot}$.

Propagation Model with Constant Speed

- Position of plasma parcel $\boldsymbol{R}(t, t_{in})$ at every moment t following its crossing of PSP at a time t_{in},

$$\boldsymbol{R}(t, t_{in}) = \boldsymbol{R}_{in}(t_{in}) + \int_{t_{in}}^{t} \boldsymbol{V}(t', t_{in})\, dt' \qquad (1)$$

where $\boldsymbol{V}(t', t_{in})$ is the plasma propagation velocity.

- Distance between the plasma parcel and the outer spacecraft,

$$d(t, t_{in}) = |\boldsymbol{R}_{out}(t) - \boldsymbol{R}_{parcel}(t, t_{in})| \qquad (2)$$

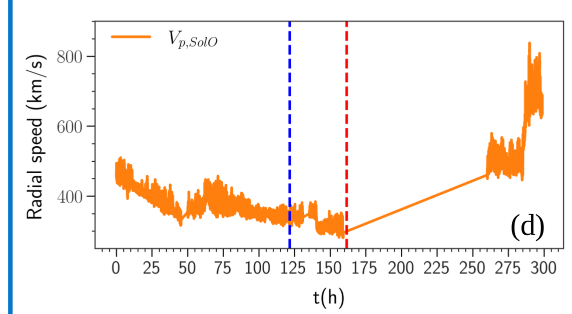

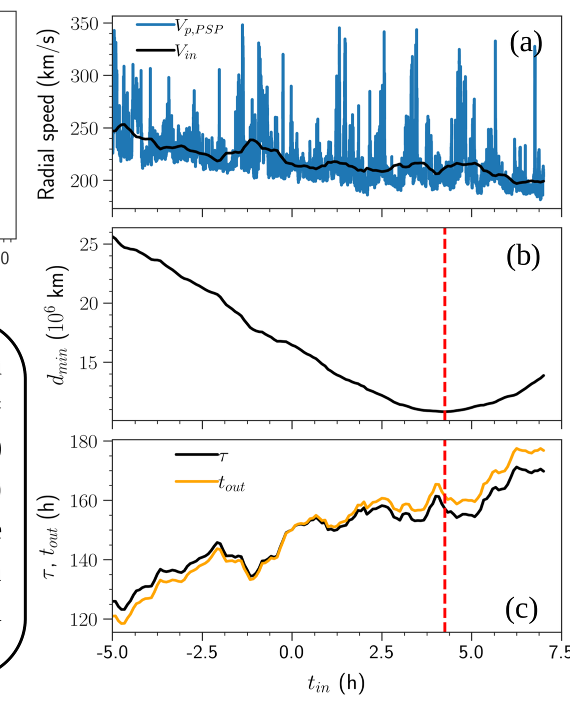

Fig. 7. Outcome of the propagation method for a radial, constant velocity V = (V_R = V_{in}, 0, 0) in RTN coordinates. (a) Radial proton speed recorded by PSP. (b) Minimum distance d_{min} between the plasma parcel and SoIO. (c) Propagation times τ and t_{out} vs t_{in}. (d) Solar wind radial speed recorded by SolO for $0 \leq t \leq 300$ h.

Even though, no matter the considered $t \in [0, 200]$ h, the **observed proton's speed at SolO is higher than at PSP**. This is consistent with results of precedent studies that reported an acceleration of the slow wind in the inner heliosphere[2,4].

Propagation Model with Constant Acceleration

- We first considered the plasma propagation with an arbitrary constant acceleration **a** constrained by measurements, then for every t_{in}, the positions and speeds of plasma parcel at every time $t > t_{in}$ following the inner spacecraft crossing are[2]:

$$\boldsymbol{R}(t) = \boldsymbol{R}_{in} + (t - t_{in})\,\boldsymbol{V}_{in} + \frac{(t-t_{in})^2}{2}\boldsymbol{a} \qquad (3)$$

$$\boldsymbol{V}(t) = \boldsymbol{V}_{in} + +(t - t_{in})\,\boldsymbol{a} \qquad (4)$$

- After the propagation, this model provides

$$\boldsymbol{R}_{out} = \boldsymbol{R}_{in} + \tau\,\boldsymbol{V}_{in} + \frac{\tau^2}{2}\boldsymbol{a} \qquad (5)$$

$$\boldsymbol{V}_{out} = \boldsymbol{V}_{in} + \tau\,\boldsymbol{a} \qquad (6)$$

with τ the propagation time, $\boldsymbol{R}_{out} = \boldsymbol{R}(t = t_{out})$ and $\boldsymbol{V}_{out} = \mathrm{V}(t = \boldsymbol{t}_{out})$.

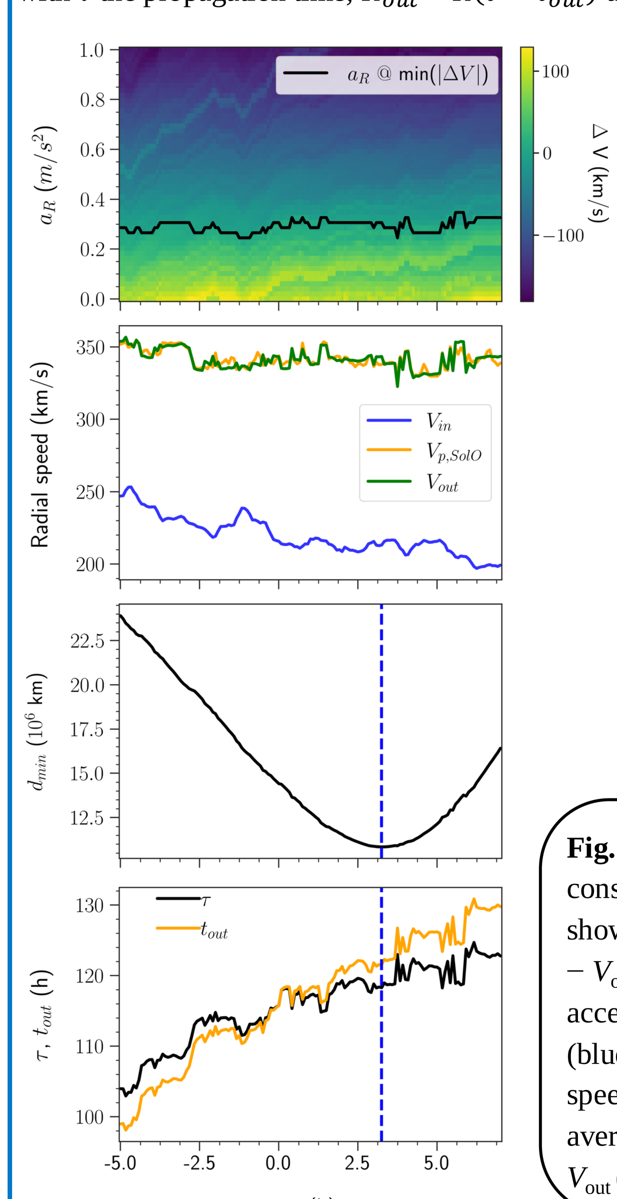

- According to constant acceleration model, t_{in} is smaller by ~ 1 h as compared to constant velocity model. Thus, the time interval to look at the inner and outer spacecraft should be respectively around $t_{in} \sim 3.25$ h (**2022-12-10 05:45:00**) and $t_{out} \sim 121.53$ h (**2022-12-15 04:02:00**).
- The **constant acceleration model implies also a significantly lower propagation time τ, by almost 40 h as compared to the constant velocity model** (as expected due to the observed increase of plasma velocity).

Fig. 8. Propagation method results using a constant acceleration $\boldsymbol{a}$. All quantities are shown as functions of t_{in}. (a) $\Delta V = \langle V_{p,SolO}\rangle - V_{out}$, and the black curve shows the radial acceleration for the minimum $|\Delta V|$. (b) V_{in} (blue), $\langle V_{p,SolO}\rangle$ (orange), the proton bulk speed measured by Solar Orbiter and averaged for Δt = 1h centered on t_{out}, and V_{out} (green). (c) d_{min}. (d) τ and t_{out}.

Same Structure Identification

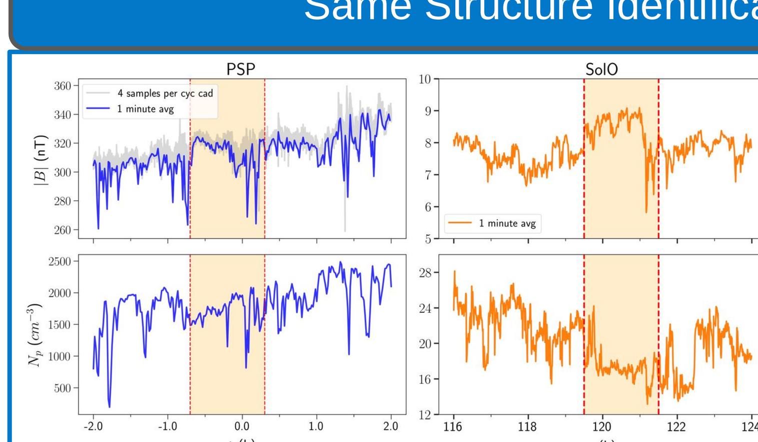

Fig. 9. Magnetic field magnitude and proton density measured by PSP and SolO around the predicted plasma line-up. Density structures are indicated between two vertical red dashed lines.

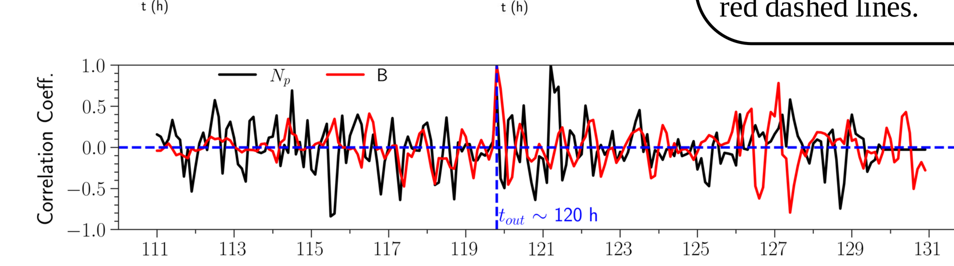

Fig. 10. Cross-correlation for measurements of the proton density N_p (black curves) and the magnetic field magnitude B (red curves) for PSP and SolO.

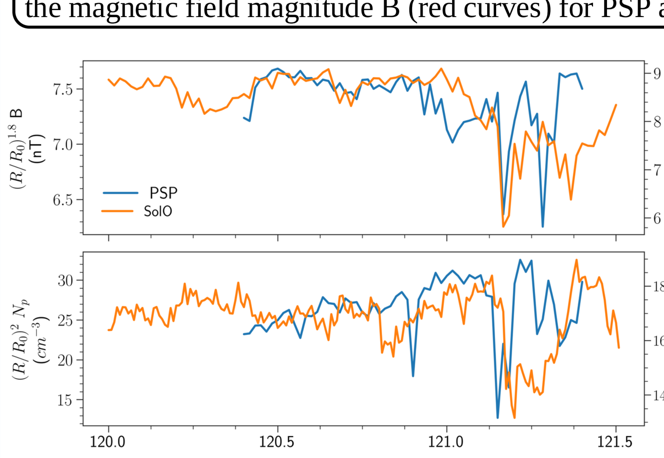

Fig. 11. Zoom-in view of the density structure observed by both PSP and SolO. (a) Proton density and (b) magnetic field magnitude, corrected by a factor $(R/R_0)^2$ and $(R/R_0)^{1.8}$, respectively, to take the expansion from PSP (blue) to SolO (orange) into account.

Results

Turbulence Anisotropy: PSD and spectral index

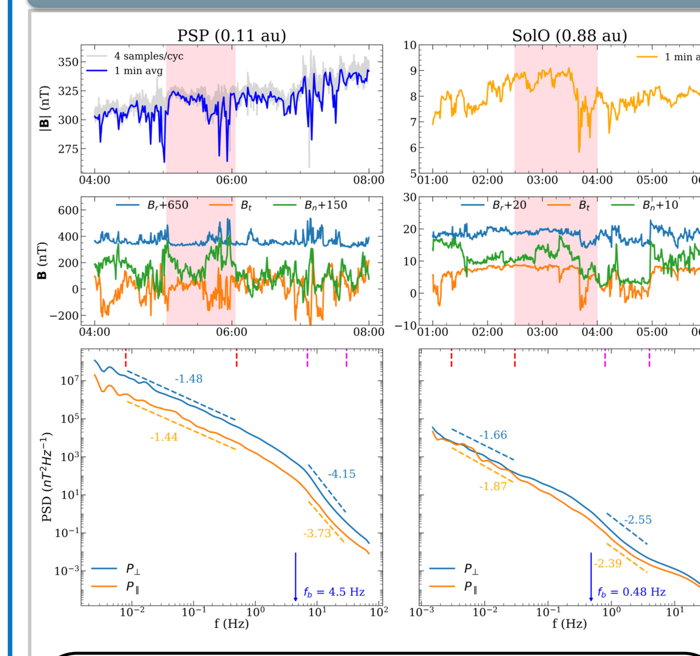

Fig. 12. The panel from top to bottom gives an overview of the magnetic field magnitude |B|, magnetic field components, and turbulence anisotropy properties (power anisotropy and spectral index anisotropy) at two distances.

- The compressibility of the solar wind turbulence continuously increases during its evolution in the heliosphere.
- The power levels systematically increase as r decreases by at least two orders of magnitude.
- At PSP, the inertial range spectral index follows -3/2 scaling, whereas at SolO position, a clear transition to -5/3 scaling is observed.
- At larger distances, the spectral break (f_b) shifts to a lower spacecraft frame frequency.

Intermittency

Structure Function, Flatness and Scaling Exponent derived from Castaing Model

- **Castaing PDF:**

$$P_{\lambda}(\delta B_l) = \frac{1}{2\pi\lambda}\int_0^{\infty} \exp\left(\frac{\delta B_l^2}{2\sigma^2}\right)\exp\left(-\frac{(\ln\sigma - \mu)^2}{2\lambda^2}\right)\frac{d\sigma}{\sigma^2},$$

where λ is a parameter that quantifies the degree of non-Gaussianity of the distribution and μ is the most probable value of the standard deviation.

- **Structure function (SF):** $S^q(\tau) = C_q \exp\left(\frac{q^2}{2}\lambda^2 + q\mu\right)$

Scaling Exponent: $\zeta(q) = \frac{q^2}{2}\frac{d\lambda^2}{d\ln\tau} + q\frac{d\mu}{d\ln\tau}$

Flatness: $F(\tau) = 3e^{4\lambda^2}$

where $C_q = \frac{(\sqrt{2})^q}{\sqrt{\pi}}\Gamma\left(\frac{1+q}{2}\right)$

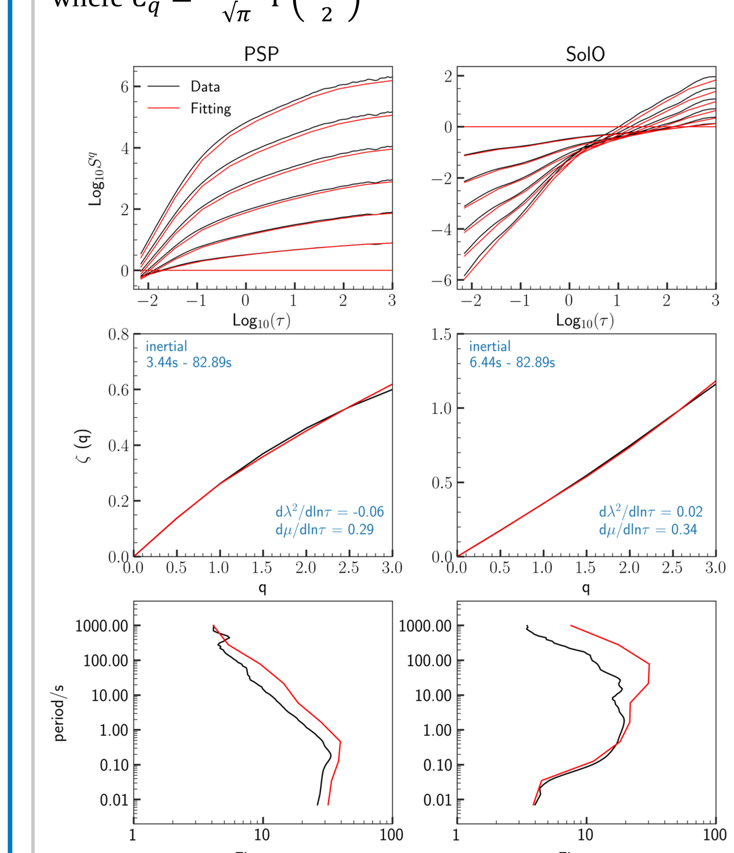

- ✓ The whole set of **SF** based on the derivation of Castaing distribution fitted very well with observational SF at both location.
- ✓ In the inertial range, the **scaling exponent $\boldsymbol{\zeta(\tau)}$** shows non-linear profile at PSP position, which represents multi-fractal scaling, whereas the SolO, $\zeta(\tau)$ has quasi-linear profile, which represents mono-fractal scaling.
- ✓ At both distances, the **flatness** profile shows a linear increase in large scales, saturation at intermediate scale, and finally a weak decrease at small scales, below MHD range.

Fig. 13. Comparison of construction results based on fitting parameters $\mu(\tau)$ and $\lambda^2(\tau)$of Castaing function (red lines) and observational results (black lines) for structure functions from order 0.5 to 3 (top panel), scaling exponent (middle panel) and flatness (bottom panel) at PSP and SolO position.

Magnetic Helicity

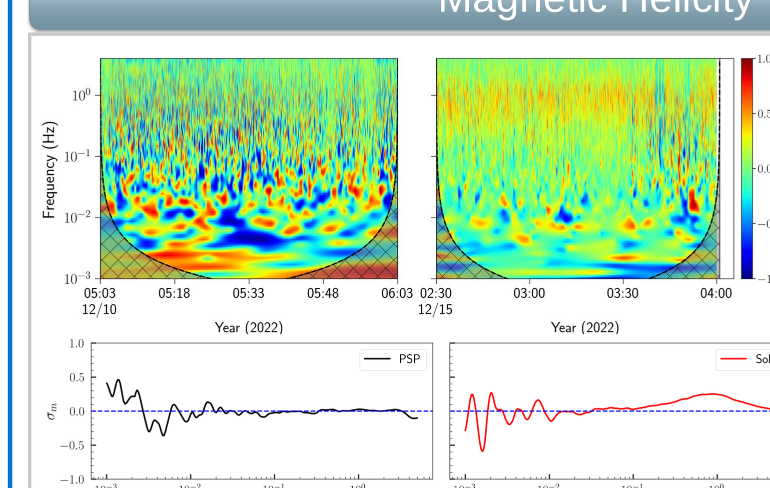

- ✓ σ_m tends to nonzero in the ion-kinetic range (around 0.1 or 1 Hz) at 0.88 au, which represents wave activity.
- ✓ wave activity almost rests at the PSP location.

Fig. 14. Normalized reduced magnetic helicity σ_m for PSP and SolO. The top panel shows the wavelet spectrogram of σ_m, and bottom panel shows time-averaged σ_m obtained from the wavelet transform. The shaded cross areas in the top panel are determined by the cone of influence (COI) during the wavelet transform.

Conclusions

1. The density structure was very stable and remained well recognizable from PSP to Solar Orbiter despite its journey of ~120 hours in the inner heliosphere.
2. The slow solar wind plasma parcel was significantly accelerated (from ~250 to ~350 km/s) during its propagation.
3. The compressibility of the solar wind turbulence continuously increases during its evolution in the heliosphere.
4. The spectral break (f_b) shifts to a lower spacecraft frame frequency increases.
5. The intermittency possess multifractal scaling at PSP and monofractal scaling at SolO as shown by the linearity profile of the scaling exponent $\zeta(q)$ of an q-order structure function.
6. The characteristics of $\frac{d\lambda^2}{d(\ln\tau)}$ in the inertial range is responsible for the feature of flatness profile over the timescale, which increases to a peak around the break, and then slightly reduces/saturates beyond the break.

References and Acknowledgements

1. Schwartz S. J., Marsch E., 1983, J. Geophys. Res. Space Phys., 88, 9919.
2. Berriot E., Démoulin P., Alexandrova O., Zaslavsky A., Maksimovic M., 2024, A&A, 686, A114.
3. Gieseler, J., Dresing, N., Palmroos, C., von Forstner, J.L.F., Price, D.J., Vainio, R. et al. 2022. Front. Astronomy Space Sci. 9.
4. Sanchez-Diaz, E., Rouillard, A. P., Lavraud, B., et al. 2016, J. Geophys. Res. Space Phys., 121, 2830.

We acknowledge the partial support of the NSF EPSCoR RII-Track-1 Cooperative Agreement OIA-1655280, NASA awards 80NSSC20K1783, 80NSSC23K0415, and a NASA IMAP subaward under NASA contract 80GSFC19C0027.